metals

MDPI

Article

Influence of the Glycidyl Azide Polymer on the Energy Release of Aluminum Sub-Micron Particles under Ultrafast Heating Rates Stimulated by Electric Explosion and Solid Laser

Yaru Li [1], Hui Ren [2] and Shuo Liu [1,*]

[1] State Key Laboratory of Precision Blasting, Jianghan University, Wuhan 430056, China; liyaru@jhun.edu.cn
[2] State Key Laboratory of Explosion Science and Safety Protection, Beijing Institute of Technology, Beijing 100081, China; renhui@bit.edu.cn
* Correspondence: liushuo@jhun.edu.cn

Abstract: Glycidyl azide polymer (GAP)-coated sub-micron aluminum (sub-mAl@GAP) particles exhibit higher heat release than their uncoated counterparts under low heating rates. However, their application in explosives has been hindered due to a lack of understanding of their energy release characteristics under heating rates of detonation levels. To address this problem, the energy release performances of sub-mAl@GAP particles under ultrafast heating rates stimulated by an electric explosion of wire and high-energy laser were studied. The results showed that the reaction of sub-mAl@GAP particles was more violent than that of an uncoated counterpart under an electric explosion stimulus. Additionally, the reaction time of the former was 0.4 ms shorter than that of the latter. In addition, the propagations of shock waves of the sub-mAl@GAP and sub-mAl were analyzed. The propagation distances of shock waves of the sub-mAl@GAP were all longer than those of sub-mAl under laser fluences of 0.5 J/cm^2, 1.2 J/cm^2, and 2.4 J/cm^2. The distance difference gradually increased with the decrease in the laser fluence. Under a laser fluence of 0.5 J/cm^2, the velocity and distance differences of the sub-mAl@GAP and sub-mAl were both the largest due to the energy contribution from the GAP. In conclusion, the fast decomposition rate of the GAP and its energy contribution would benefit the energy release of sub-mAl under ultrafast heating rates.

Keywords: explosives; electric explosion; energy release; laser stimulus; glycidyl azide polymer

check for updates

Citation: Li, Y.; Ren, H.; Liu, S. Influence of the Glycidyl Azide Polymer on the Energy Release of Aluminum Sub-Micron Particles under Ultrafast Heating Rates Stimulated by Electric Explosion and Solid Laser. *Metals* **2024**, *14*, 786. https://doi.org/10.3390/met14070786

Academic Editor: Giuseppe Lacidogna

Received: 26 May 2024
Revised: 28 June 2024
Accepted: 3 July 2024
Published: 5 July 2024

Copyright: © 2024 by the authors. Licensee MDPI, Basel, Switzerland. This article is an open access article distributed under the terms and conditions of the Creative Commons Attribution (CC BY) license (https://creativecommons.org/licenses/by/4.0/).

1. Introduction

An aluminum (Al) particle is one of the most widely used metals in the energetic fields such as batteries, hydrogen energy, propellants, and explosives [1–5]. Studies on the reaction behavior of Al particles have attracted numerous attention over the last few decades [6–10]. The high energy density of Al particles is the key factor, and they are employed in the energetic fields. However, the energy release behavior of Al particles can be impacted by their physical property (shape, size, and the state of the oxide shell), heating stimuli, and the state of the oxidant. Particularly, the energy release rate of Al particles will significantly influence the energy release efficiency and the blast effects of the explosive composites.

Unlike the steady combustion state of the propellant, the atmosphere in the post-detonation area is more complicated and raises a higher challenge for the study of Al reaction. The temperature of detonation products could rise to 2000~4000 K in nanoseconds when an explosive is detonated. Additionally, the detonation pressure is also elevated to tens of GPa at the same time [11]. The reaction mechanisms of the metals will be totally changed under such a complex thermodynamic environment [12,13]. To date, there is still an unsolved and interesting mystery that challenges all researchers: what interaction happens between Al particles and the detonation products in the post-detonation area? Based on the detonation characteristics of aluminized explosives, an empirical theory for

the reaction of Al particles has been built on the detonation model of ideal explosives. According to this theory, the reaction of the Al particle does not happen until the expansion of detonation products, which results in a long sequential reaction zone [14–16]. Therefore, aluminized explosives will produce more detonation heat but smaller detonation velocity than explosives without Al particles.

However, recent studies showed that sub-micron Al (sub-mAl) particles could take part in the reaction in the Chapman–Jouguet plane and result in a higher detonation pressure. Zhang et al. [17] employed an explosive device of a long pipeline to study the detonation pressure of the sub-micron aluminized explosives. The results showed that the detonation pressure of sub-micron-aluminized explosives was 3~4 times as much as that of micron-aluminized explosives. Additionally, Hu et al. [7] found that around 80% of sub-mAl particles could react in the detonation zone, and the peak pressure of the shock wave of sub-micron aluminized CL-20 (hexanitrohexaazaisowurtzitane) explosives was significantly higher than that of micron-aluminized CL-20 explosives. In addition, Elbasuney et al. [18] compared the detonation properties of TNT (2,4,6-trinitrotoluene) explosives containing sub-mAl particles and mAl particles. The workability of TNT was elevated by 48% by sub-mAl and only 17% by mAl. They also found that TNT explosives containing sub-mAl particles could not only decrease the critical detonation diameter of TNT but also increase the detonation velocity by 680 m/s.

The oxidation of Al particles would be severer when their size reduces to a sub-micron scale, which will harm their active content after long-term storage. To protect the active content of sub-mAl particles, organic polymers, metals, and carbon materials are employed to coat their surface. Among them, polymers could achieve intact cover due to good flexibility and good mechanical properties. More recently, energetic polymers have attracted considerable attention due to their high energetic property and good compatibility with explosives. The glycidyl azide polymer (GAP) is a new kind of energetic binder and has higher energy density than nitrocellulose (NC). Zeng et al. [19] employed the GAP to coat the surface of Al particles. They found that the stability and flowability of the resulting Al particles were greatly improved, and the particles showed good compatibility with the LLM-105 [20]. Lima et al. [21] grafted a GAP on the surface of Al particles, and combustion tests showed that the combustion of Al particles would be more complete and a higher combustion heat would be acquired with the help of a GAP. Our previous work proved that a GAP coating could improve the hydrophobicity of Al particles and increase the stability in long-term storage [22].

To date, studies on the GAP-coated sub-mAl particles have been limited by their combustion performance under slow heating rates (~1000 °C/s). Their combustion performances under heating rates of a detonation level (~10^{10} °C/s) have not yet been well understood. In this work, we used solid laser and electric explosion strategies to achieve high heating rates. The energy release performance of GAP-coated sub-mAl (sub-mAl@GAP) particles was thoroughly studied. The duration of the laser pulse was 6 ns. The energy fluence of each pulse was over one billion W/cm^2. The plasma of thousands of Kelvins will be excited when the laser irradiates on the surface of materials (energetic or inert) [23,24]. Consequently, shock waves will be induced and propagate radically forward. The propagation velocity of the shock wave is dependent on the energy released from the materials. Therefore, it is a feasible strategy to evaluate the energy release of fuel particles and their mixtures with polymers at the detonation and post-detonation timescales [24–26]. The energy release process of the electrical explosion can be completed on the nanosecond scale, and the peak temperature of the metal plasma after the electric explosion can reach up to 10^5 °C by changing the circuit and wire parameters [27,28]. The heating rate of the electric explosion is comparable to that of the detonation process. Based on the above principle, the rapid heating process has been realized by the electric explosion of metal wire technology, and the thermal response behaviors of sub-mAl@GAP particles under high heating rates were investigated.

2. Experimental

2.1. Materials and Characterizations

The sub-mAl@GAP particles with 16.7 wt.% of the GAP were manufactured by the in situ coating strategy, and detailed procedures are described in Section SI.1 in the Supplementary Materials. Additionally, the physical and chemical properties of the Al and GAP were listed in Table S1 in the Supplementary Materials. The morphology of the sub-mAl@GAP particles was observed by a transmission electron microscope (TEM, Tecnai G2 F20, FEI Co., Hillsboro, OR, USA). The thermodynamic studies of the samples were characterized by means of differential scanning calorimetry (DSC) using a thermal analyzer (STA 449 F3, NETZSCH, Co., Selb, Germany) under an airflow of 50 mL/min. The tests were carried out in Al_2O_3 crucibles with pinhole covers at heating rates of 5 °C/min, 10 °C/min, and 20 °C/min. As a comparison, the uncoated sub-mAl particles were also characterized under the same conditions.

2.2. Combustion Characterization of the Sub-mAl@GAP Stimulated by an Electric Explosion

Figure 1 presents a schematic diagram and corresponding photo of the experimental device of an electric explosion. For each test, 0.500 ± 0.003 g of samples were loaded into a low-density polyethylene mold with a length of 40.00 mm and an inner diameter of 7.00 mm. The diameter of the Al wire was 0.30 mm, which was placed in the center of the sample cylinder. The Al wire is supplied with an external energy storage capacitor with a capacity of 0.4 μF and a voltage of 22 kV, and the power supply circuit is shown in Figure 2. The inside pressure of the reaction chamber was controlled by a pressure transmitter. The reaction process was recorded by a high-speed camera (CP70-1HS-M-1900, Optronis, Kehl, Germany) at a rate of 10,000 fps. The exposure time of each frame of the photo was set to 0.1 ms. As a comparison, the uncoated sub-mAl particles were also characterized under the same conditions.

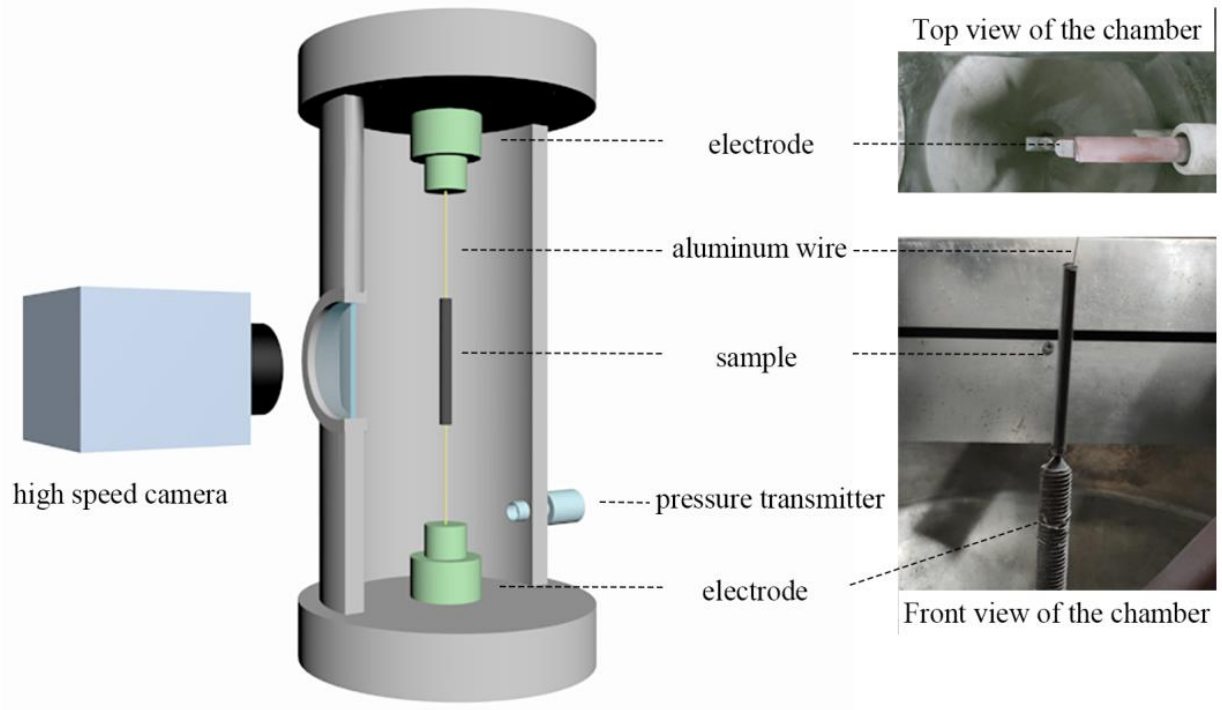


Figure 1. A schematic diagram and the corresponding picture of the set-up of the electric explosion.

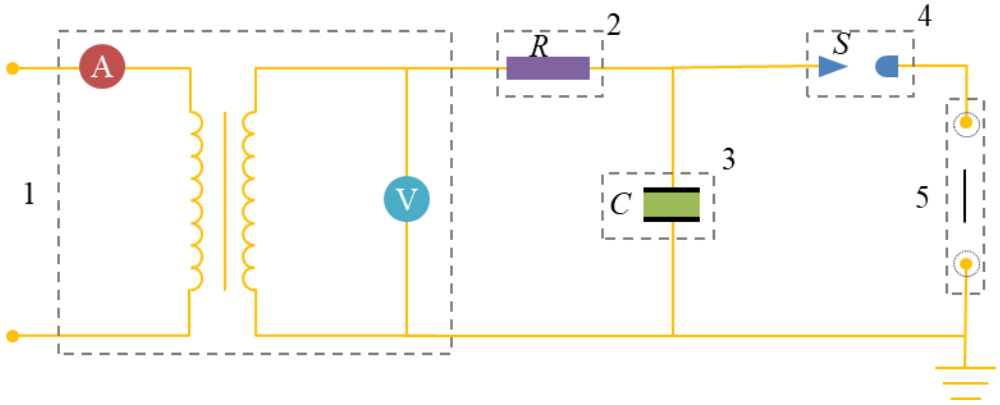


Figure 2. A schematic diagram of the power supply circuit for the electric explosion experiment (1 is the high-voltage power supply; 2 is the resistance of the circuit; 3 is the capacitance; 4 is the switch; 5 is the discharge electrode).

In the detonation environment, the detonation products participating in the oxidation reaction of Al particles are in the form of fully heated gaseous products. Under such high temperatures, the gaseous products will be ionized, which is significantly different from the ordinary surrounding air molecules under slow heating conditions. To simulate the detonation environment, the presence of high-temperature gas products is necessary. An ammonium oxalate molecule ($(NH_4)_2C_2O_4$) is like an explosive molecule that contains four elements: C, H, O, and N. The thermal decomposition formula of ammonium oxalate is shown in Equation (1), in which decomposition products are very close to the composition of explosive detonation products in Equations (2)–(4). In the equations, RDX and HMX refer to hexogen and octogen, respectively. In addition, the thermal decomposition temperature of ammonium oxalate is only 95 °C, and it can quickly decompose and produce numerous high-temperature ion fragments under the impact of high energy from an electric explosion. For each test, the sample was mixed with ammonium oxalate at a mass proportion of 2:3.

$$\text{Ammonium oxalate}: (NH_4)_2C_2O_4 \rightarrow CO\uparrow + CO_2\uparrow + 3H_2O\uparrow + 2NH_3\uparrow; \quad (1)$$

$$\text{RDX}: C_3H_6N_6O_6 \rightarrow 3CO\uparrow + 3H_2O\uparrow + 3N_2\uparrow; \quad (2)$$

$$\text{TNT}: C_7H_5N_3O_6 \rightarrow 3.5CO\uparrow + 2.5H_2O\uparrow + 1.5N_2\uparrow + 3.5C; \quad (3)$$

$$\text{HMX}: C_4H_8N_8O_8 \rightarrow 4CO\uparrow + 4H_2O\uparrow + 4N_2\uparrow. \quad (4)$$

2.3. Combustion Characterization of the Sub-mAl@GAP Stimulated by a Laser

The combustion characterization of the sub-mAl@GAP stimulated by a laser was achieved by a Schlieren system [29]. An Nd:YAG laser (1064 nm, InnoLas Laser, Krailling, Germany) was used to initiate the reaction of sub-mAl@GAP particles. The pulse duration of the laser was 6 ns. The diameter of the laser beam was 6 mm. The laser fluence was determined by the measured pulse energy and the spot diameter. A flash lamp system (JML-C2, Rapp OptoElectronic, Wedel, Germany) served as the background light for the Schlieren system. A 75 mm lens was used in the Schlieren system to detect the density change in the reaction field. A high-speed camera (SIMD8, Specialized Imaging Ltd., Pitstone, UK) was employed to record the propagation history of the laser-induced shock wave. The shooting rate was 952,381 fps with a duration of 50 ns for each frame. The system was triggered by a pulse generator (DG535, Stanford Research Systems, Inc., Sunnyvale, CA, USA) under the precise time delay measured by an oscilloscope (DPO7104, Tektronix, Beaverton, OR, USA). The time jitter for the delay system was within 2 ns. The energy output of the laser was measured by an energy meter (J-50MB-YAG, Coherent, Saxonburg, PA, USA). Three different laser fluences, i.e., 2.4 J/cm^2, 1.2 J/cm^2, and 0.5 J/cm^2, were applied to the samples to better understand their performances. For each test, the

sample adhered to the mold surface by a dual adhesive tape. Each sample was tested three times under the same condition. The experiment setup is shown in Figure S1 in the Supplementary Materials. As a comparison, uncoated sub-mAl particles were also characterized under the same conditions.

3. Results and Discussion

3.1. Morphological Characterizations of Sub-mAl@GAP Particles

The morphologies of sub-mAl@GAP particles characterized by TEM are shown in Figure 3a,b, in which Figure 3b is the partially enlarged image of Figure 3a. To make a comparison, the morphologies of sub-mAl particles were also characterized by TEM. The results are displayed in Figure 3c,d. Figure 3d is the partially enlarged image of Figure 3c. It could be learned from Figure 3a that sub-mAl@GAP particles were in the shape of a sphere with a diameter smaller than 200 nm. There was no significant increment in particle size after coating when comparing them with the size of the sub-mAl particles in Figure 3c. It could be seen in the enlarged image of Figure 3b that there were two layers outside the Al particles. Additionally, the inner layer was much thinner than the outside layer. The outside layer was much more transparent than the inner layer. According to the observation principle of the TEM, the transparency of a material was determined by its thickness and atomic number. The number of Al atoms was larger than those of atoms composed of the GAP. Additionally, by comparing them with the layers of the sub-mAl particles in Figure 3d, it could be identified that the inside layer was the inherent aluminum oxide. In addition, the oxide layer of the sub-mAl@GAP particles was relatively thinner than the GAP layer, indicating effective protection of active Al.

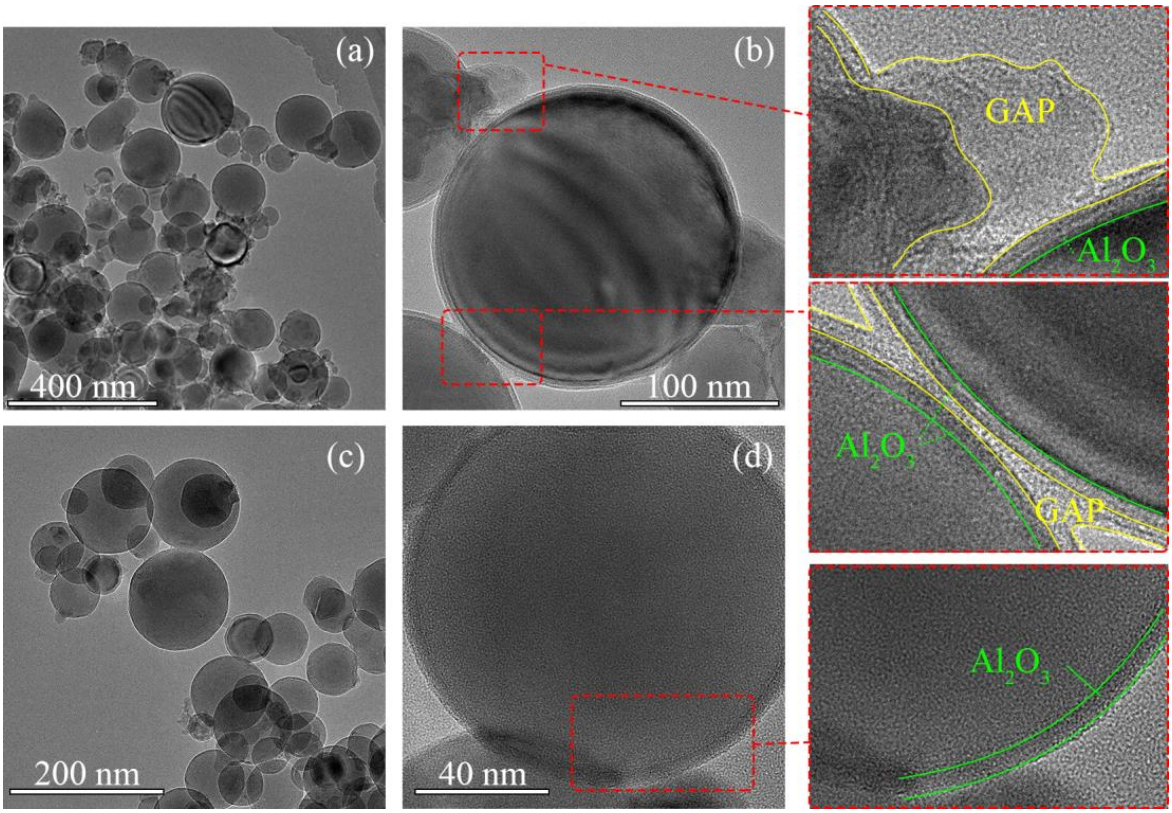


Figure 3. TEM images of sub-mAl@GAP (**a**,**b**) and sub-mAl particles (**c**,**d**).

3.2. Thermal Reaction Kinetics of the Sub-mAl@GAP

To understand the reaction kinetics of the sub-mAl@GAP, both thermographs of the sub-mAl@GAP, GAP, and sub-mAl at different heating rates were studied, and the corresponding DSC curves are shown in Figure 4. Figure 4a,c present the DSC curves of

the sub-mAl@GAP in the ranges of 100 °C to 400 °C and 510 °C to 650 °C. It could be learned from Figure 4a,b that the exothermic peak temperatures (T_p) of the sub-mAl@GAP (Figure 4a) were 242.2 °C, 251.9 °C, and 262.3 °C at heating rates of 5 °C/min, 10 °C/min, and 20 °C/min, which were ~2 °C lower than those of the GAP (Figure 4b), indicating a change in the reactivity of the GAP. To quantitively study the interaction between sub-mAl and the GAP, the activation energy (*Ea*) of the sub-mAl@GAP and GAP were calculated by the Kissinger method [30] and Ozawa method [31] based on the T_p and their corresponding heating rates (β) in Figure 4. Table 1 lists the kinetic parameters of the exothermic reaction of the sub-mAl@GAP and GAP. The *Ea* of the sub-mAl@GAP acquired by the Kissinger method and Ozawa method were 149.48 kJ/mol and 150.46 kJ/mol, respectively. Meanwhile, those of the GAP were 174.25 kJ/mol and 174.00 kJ/mol. The fitting coefficients for both samples were above 0.9846, indicating good fitting results. The results showed that the *Ea* of the sub-mAl@GAP at this stage was significantly lower than that of the GAP. The difference between them was as large as 24.77 kJ/mol with respect to the results of the Kissinger method. In conclusion, the decomposition of the GAP proceeded more easily under the influence of sub-mAl.

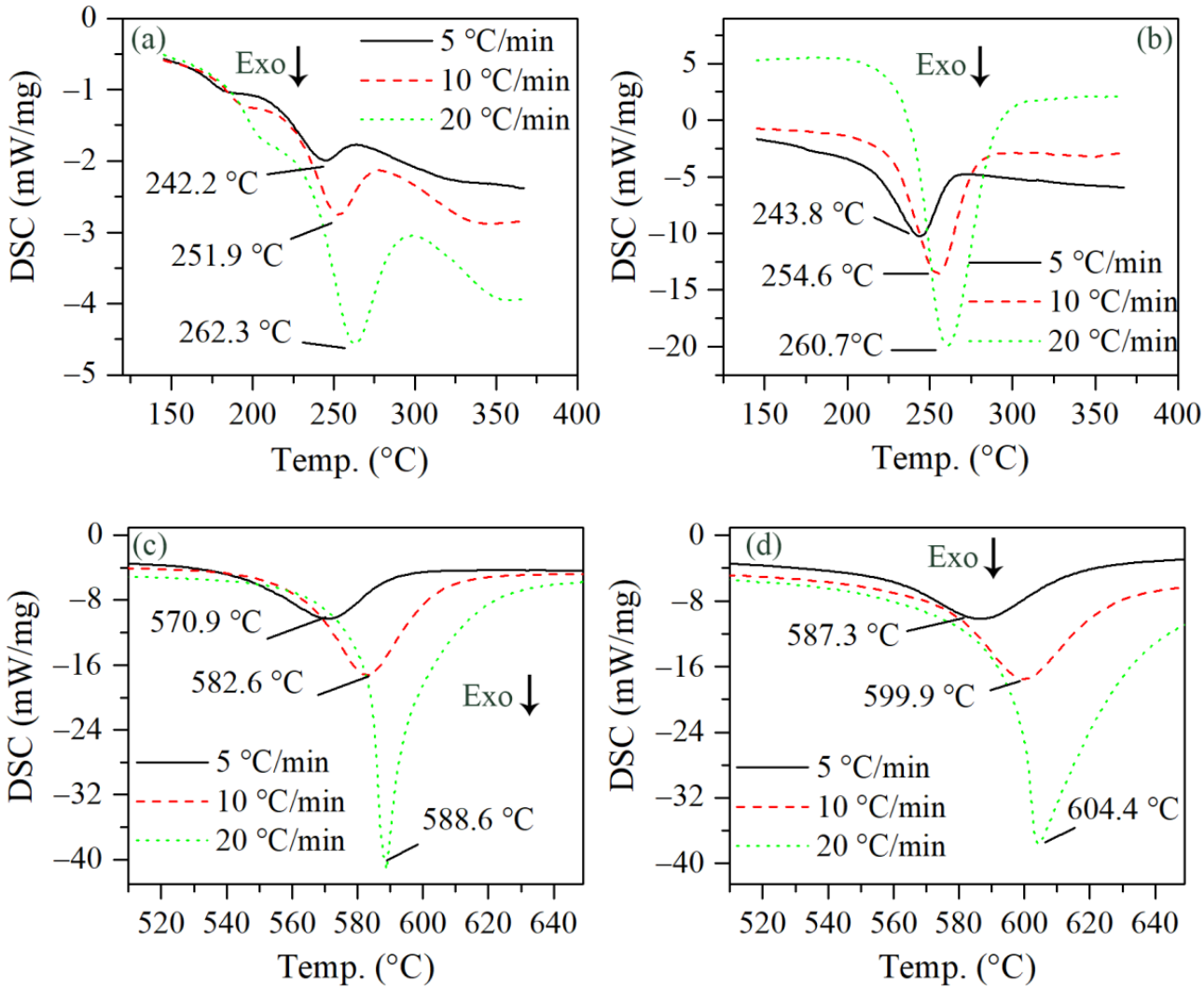


Figure 4. DSC curves of the sub-mAl@GAP (**a**,**c**), GAP (**b**), and sub-mAl (**d**) at heating rates of 5 °C/min, 10 °C/min, and 20 °C/min. (Temperature range: **a**, 100~400 °C; **c**, 510~650 °C.).

Table 1. Kinetic parameters of the exothermic reaction of the sub-mAl@GAP, GAP, and sub-mAl.

Samples	Kissinger Method			Ozawa Method	
	E_a/(kJ/mol)	lg(A/s^{-1})	R	E_a/(kJ/mol)	R
sub-mAl@GAP [a]	149.48	12.90	0.999959	150.46	0.999951
GAP	174.25	15.40	0.986003	174.00	0.984634
sub-mAl@GAP [c]	442.74	25.17	0.982194	434.50	0.981083
sub-mAl	458.02	25.57	0.963496	449.28	0.961308

Note: a and c, respectively, stand for the cases in Figure 4a,c.

In addition, the T_p of the oxidation of the sub-mAl@GAP (Figure 4c) were 570.9 °C, 582.6 °C, and 588.6 °C, which were lower than the T_p of sub-mAl (Figure 4d) at corresponding heating rates. The decreases in the T_p were 16.4 °C, 17.3 °C, and 15.8 °C under heating rates of 5 °C/min, 10 °C/min, and 20 °C/min, respectively. Furthermore, the E_a of the sub-mAl@GAP acquired by Kissinger method and Ozawa method were 442.74 kJ/mol and 434.50 kJ/mol. On the contrary, the E_a of sub-mAl acquired by the Kissinger method and Ozawa method were 15.28 kJ/mol and 14.78 kJ/mol higher than those of the sub-mAl@GAP, respectively. It could be concluded that the GAP coating could significantly decrease the activation energy of sub-mAl oxidation and facilitate the oxidation process.

3.3. Reaction Performance of the Sub-mAl@GAP Stimulated by an Electric Explosion

Figure 5 presents high-speed photographs of the combustion processes of the sub-mAl@GAP and sub-mAl particles under a heating stimulus of an electric explosion. After the electric explosion, the temperature of the Al wire would reach a point higher than the boiling point of alumina (2980 °C). Consequently, the Al wire would be ionized. The sample was rapidly heated. Under such conditions, the ammonium oxalate decomposed into high-temperature ion fragments. Meanwhile, there was still energy left from the electric explosion after initiating the reaction of sub-mAl particles. Therefore, the shining light in the photo was contributed by three parts: Al plasma from the electric explosion, ion fragments of ammonium oxalate, and the combustion flame of Al. Although bright light was emitted by both the sub-mAl and sub-mAl@GAP particles, the shape of the light was significantly different from each other. The light irradiation from sub-mAl was uniformly distributed along the axial direction. However, that from the sub-mAl@GAP was radially irradiated. It indicated the reaction of sub-mAl@GAP particles was much more violent than that of sub-mAl particles due to the immediate release of active Al particles after the decomposition of the GAP. Therefore, the reaction of Al was initiated much earlier and led to a higher heat release. This could also be proven by the fact that it only took sub-mAl@GAP particles 1.8 ms to finish the reaction; on the contrary, the reaction time of sub-mAl was much longer (2.2 ms). Meanwhile, the light emitted from the reaction of sub-mAl@GAP particles was much brighter than that of sub-mAl particles at the same time, indicating an improvement in the reaction rate of sub-mAl particles owing to the help of GAP coating.

3.4. Energy Release of the Sub-mAl@GAP Stimulated by a Laser

3.4.1. Influence of the Laser Fluence on the Energy Release of the Sub-mAl@GAP

To study the influence of the laser fluence on the propagation process of laser-induced shock waves of the sub-mAl@GAP, the propagation processes of shock waves under three characteristic laser fluences of 2.4 J/cm^2, 1.2 J/cm^2, and 0.5 J/cm^2 were measured, and the results are shown in Figure 6. The propagation distance of the shock wave increased with the increase in the laser fluence. Meanwhile, the propagation differences between shock waves under stimuli of adjacent laser fluences gradually increased with time. In the beginning, the distance difference between shock waves induced by laser fluences of 0.5 J/cm^2 and 1.2 J/cm^2 was 0.4 mm, and those induced by laser fluences of 1.2 J/cm^2 and 2.4 J/cm^2 was 0.3 mm. The former difference was larger than the latter difference. With time increased to 12.35 μs, the distance difference became 1.5 mm and 1.6 mm, which were

3.8 and 5.3 times as large as those in the beginning, respectively. The former difference was lower than the latter difference. The situation was completely inverted to the opposite. It reflected the laser energy absorbed in the plasma or stored in the vapor played a major role in the early stage of the shock wave propagation. Therefore, the higher the laser fluence, the farther the propagation distance of the initial shock wave. The energy stored behind the shock wave front was simply the heat generated by laser interactions with the materials when the laser fluence was lower than the critical ablation threshold (1.2 J/cm^2) of sub-mAl. Al vapor would be ionized if the laser fluence was higher than 1.2 J/cm^2, which would result in more laser energy absorption by the plasma. Therefore, the energy stored in the vapor was significantly elevated when the laser fluence reached 1.2 J/cm^2. Consequently, in the beginning, the distance difference of shock waves induced by 1.2 J/cm^2 and 2.4 J/cm^2 was smaller than that induced by 1.2 J/cm^2 and 0.5 J/cm^2. The energy supported the subsequent propagation of the shock wave was mainly laser energy stored in the plasma for the situation with 2.4 J/cm^2, reaction energy of the sub-mAl@GAP for the case of 0.5 J/cm^2, and laser energy in the beginning and reaction energy taking charge later for the phenomenon of 1.2 J/cm^2. This led to the propagation difference between 1.2 J/cm^2 and 2.4 J/cm^2, which gradually increased and eventually exceeded that between 0.5 J/cm^2 and 1.2 J/cm^2.

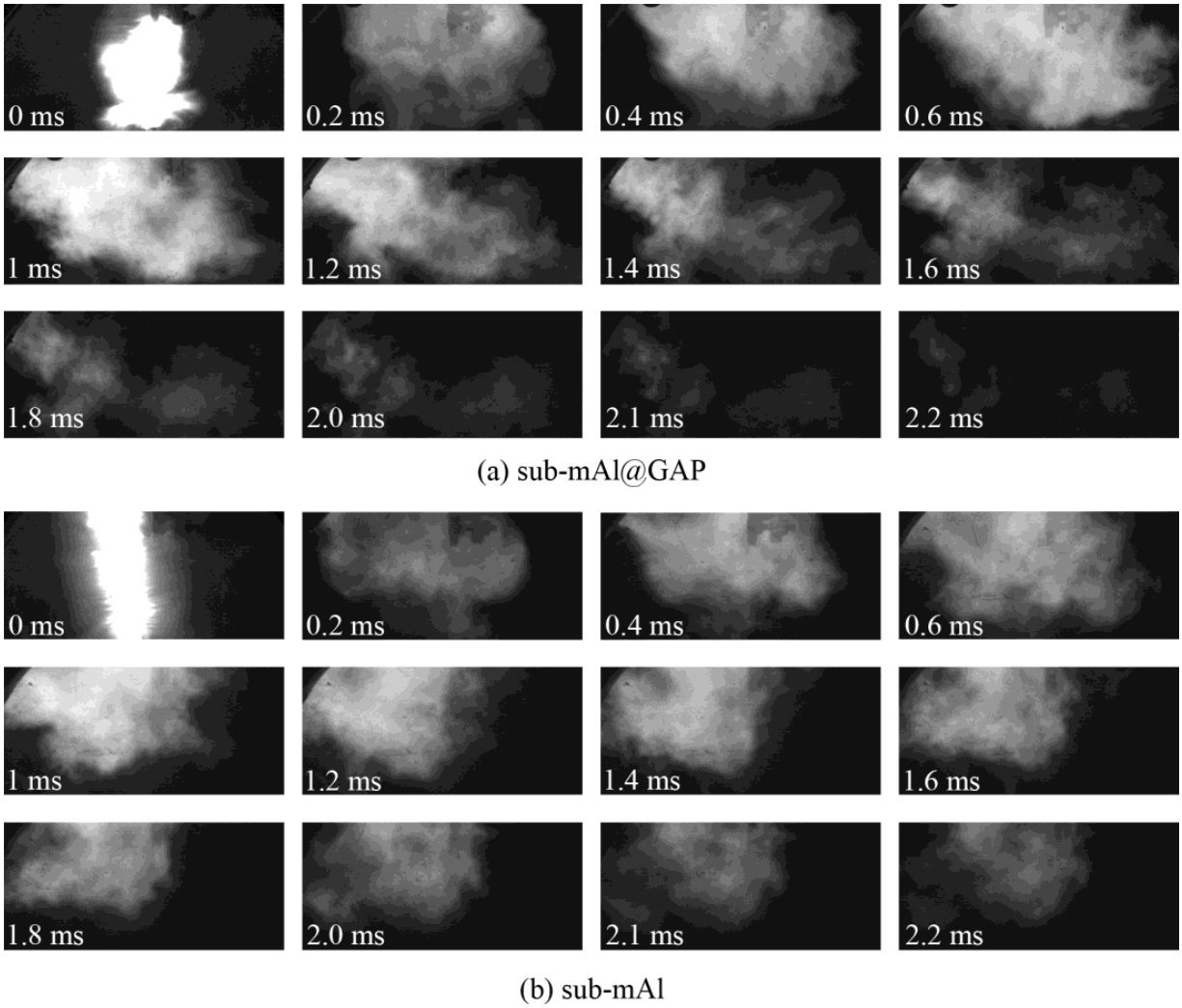


Figure 5. Reaction process of the sub-mAl@GAP (**a**) and sub-mAl (**b**) under the heating stimulus of an electrical explosion.

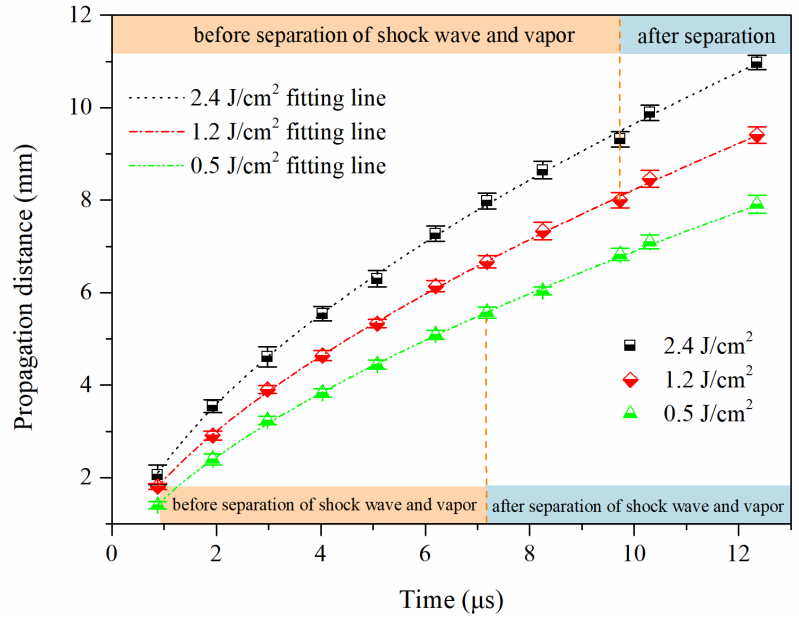


Figure 6. Variation of the propagation distances of sub-mAl@GAP shock waves with time under different laser fluences.

According to the research by McKay and Nánai [32,33], the propagation distance ($s(t)$) of a shock wave is exponentially related to time (t), as depicted in Equation (5). The propagation distance of shock waves of the sub-mAl@GAP varied with time under three different laser fluences, which were fitted according to this theory, and the fitting curves are also plotted in Figure 7. The corresponding fitting parameters are listed in Table 2.

$$s(t) = s_0 + at^b \quad (5)$$

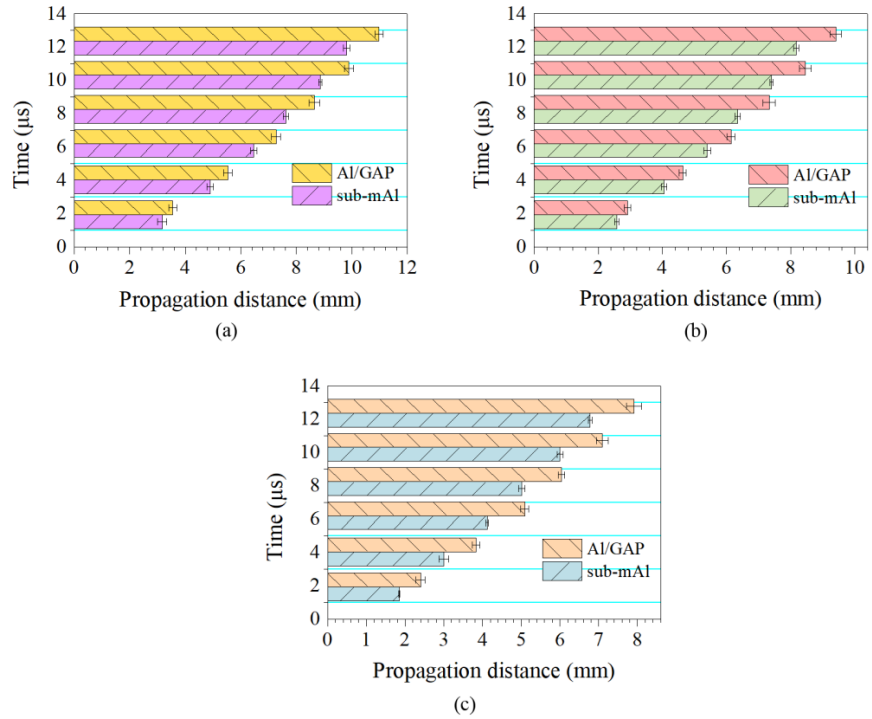


Figure 7. Shock wave propagation distance of the sub-mAl@GAP and sub-mAl over time under laser fluences of (**a**) 2.4 J/cm^2, (**b**) 1.2 J/cm^2, and (**c**) 0.5 J/cm^2.

Table 2. Fitting parameters related to the time-dependent propagation distance of the shock wave.

Laser Fluence/(J/cm^2)	s_0	a	b	R
2.4	−0.3374	2.62381	0.5806	0.99904
1.2	0.05504	1.90184	0.6333	0.99962
0.5	−0.07697	1.62728	0.6319	0.99937

In the equation, $s(t)$ is the propagation distance of the shock wave front, mm; t is the propagation time, μs; and s_0, a, and b are parameters that need to be determined based on specific situations. It could be concluded from Table 2 that the exponents (b) were 0.5806, 0.6333, and 0.6319 for the cases with laser fluences of 2.4 J/cm^2, 1.2 J/cm^2, and 0.5 J/cm^2. The correlation coefficients were all above 0.999, indicating that the fitting results were consistent with the theory of McKay and Nánai [32,33].

3.4.2. Influence of the GAP on the Energy Release of the Sub-mAl@GAP

To make a comparison, the variation difference of propagation distances of the shock waves of the sub-mAl@GAP and sub-mAl over time under three laser fluences were analyzed, and the results are shown in Figure 7. It could be concluded that the propagation distances of the shock waves for both samples increased with the increase in the laser fluence over the period. Additionally, the propagation distance of the shock wave from the sub-mAl@GAP was longer than that from sub-mAl under the same laser fluence, and the difference gradually increased over time. In the case of a laser fluence of 2.4 J/cm^2, the traveling difference of the shock wave increased from 0.4 mm at 1.93 μs to 1.2 mm at 12.35 μs. The difference under a laser fluence of 1.2 J/cm^2 elevated 0.9 mm over the same period. In addition, the greatest distance difference at 1.93 μs was achieved under 0.5 J/cm^2. The propagation distance of the sub-mAl@GAP was 0.6 mm longer than that of sub-mAl. The reason for such a big difference could be explained by the Schlieren results in Figure 8.

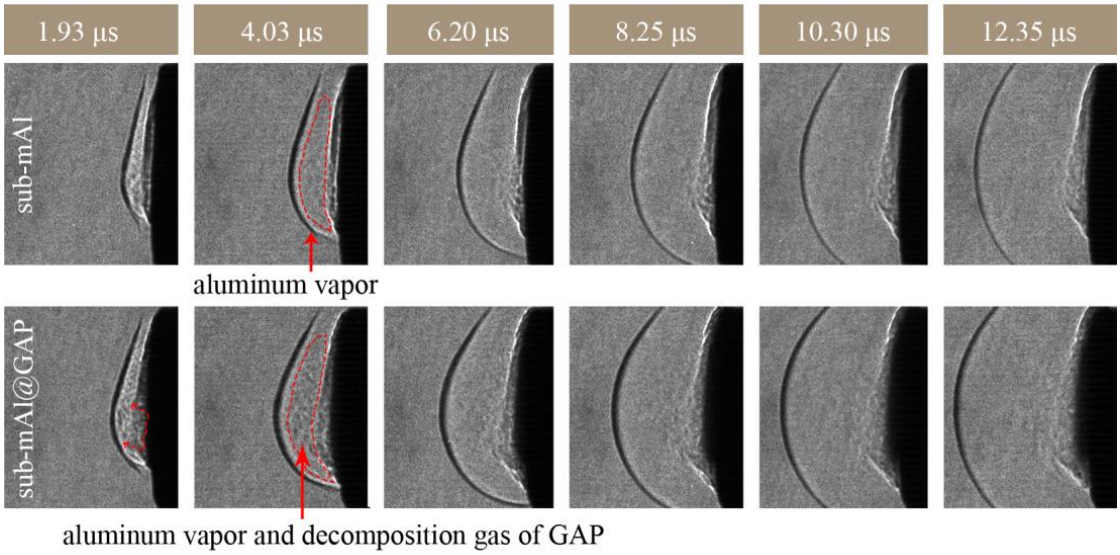


Figure 8. Schlieren picture of the shock wave propagation of the sub-mAl@GAP and sub-mAl at a laser fluence of 0.5 J/cm^2.

Figure 8 provides the Schlieren picture of shock wave propagation of sub-mAl@GAP and sub-mAl under laser fluences of 0.5 J/cm^2. At 1.93 μs, the gas density behind the shock wave front of the sub-mAl@GAP was significantly higher than that of sub-mAl, indicating the generation of gaseous products from the sub-mAl@GAP. The gaseous products are ejected toward the laser direction, as indicated by the red dashed arrow. The amount of pure Al vapor was not high under this laser energy density according to the Schlieren

picture of sub-mAl in Figure 8. Therefore, the gaseous products generated from the sub-mAl@GAP were the combined results of Al vapor and decomposition products of the GAP. The decomposition temperature of the GAP was far lower than the melting point of Al (Table S1). As a result, the GAP could achieve complete decomposition as the temperature of Al underwent melting and vaporization. Meanwhile, a large number of gaseous products and heat would be produced during decomposition, which significantly assisted the development of shock waves. The concentration of gas from the sub-mAl@GAP (in the red circle area) remained at a high level until 4.03 μs, and that of sub-mAl had already decreased. Under such conditions, the pressure behind the shock wave front of the sub-mAl@GAP was significantly higher than that of sub-mAl. Hence, the propagation velocity of the former was higher than that of the latter. Therefore, there was a remarkable difference in the propagation distances of shock waves between sub-the mAl@GAP and sub-mAl over the early period. Under a higher laser fluence, the difference in the propagation distance between them was reduced. This was because the amount of Al vapor induced by the high laser fluence was enough to support the following propagation of the shock wave. As a result, the additional assistance effect from the GAP was not that noticeable anymore.

The propagation velocity of the shock wave could be determined by the energy release rate of the particles. Therefore, the level of energy supply to the shock wave could be evaluated by measuring the propagation velocity of the shock wave [34]. The relationship of the propagation velocity $u(t)$ and time (t) could be obtained by differentiating $s(t)$ with respect to t, as shown in Equation (6).

$$u(t) = abt^{b-1} \tag{6}$$

In the equation, $u(t)$ is the propagation velocity of the shock wave front, mm/μs.

Based on the fitting parameters in Table 2 and Equation (6), the variations of propagation velocities of shock waves of the sub-mAl@GAP with time under different laser fluences could be acquired, as shown in Figure 9a. According to Figure 9a, the propagation velocities of the shock waves increased with the increase in the laser fluence. The initial propagation velocities of shock waves from the sub-mAl@GAP were 1.6 mm/μs, 1.3 mm/μs, and 1.1 mm/μs under laser fluences of 2.4 J/cm^2, 1.2 J/cm^2, and 0.5 J/cm^2, respectively. The propagation velocities of the shock waves decreased over time, which could be divided into three stages based on the slope of the curve and Schlieren images. The first stage ranged from 0.88 μs to 2.98 μs, during which period the thermal energy stored in plasma/vapor was converted into kinetic energy. With the generation and propagation of shock waves, energy was quickly consumed, which led to an immediate loss in the propagation velocity. The second stage ranged from 2.98 μs to 7.18 μs, during which stage the velocity of the shock wave descended at a slower rate than before. This was because the released energy from the chemical reaction of the sub-mAl@GAP replenished the energy supporting the shock wave, which slowed down the temperature drop in the sub-mAl@GAP plasma [35]. At the beginning of the last stage, the velocity differences between adjacent energy fluences were the same. After that, the velocity difference between 2.4 J/cm^2 and 1.2 J/cm^2 gradually decreased due to the faster attenuation of velocity in the case of 2.4 J/cm^2.

The fast attenuation of the velocity for 2.4 J/cm^2 was because the propagation of the shock wave needed to consume more energy to overcome the air resistance. The deceleration rates of the shock waves at laser fluences of 1.2 J/cm^2 and 0.5 J/cm^2 were the same, which proved that their subsequent shock wave propagation mainly depended on the energy release of chemical reactions. In addition, for the case of 0.5 J/cm^2, the shock wave front was separated from the vapor after 7.18 μs (Figure 6); after that, the propagation velocity of the shock wave gradually attenuated due to lack of energy supply and air resistance. Additionally, the propagation velocity of the shock wave under a laser fluence of 1.2 J/cm^2 was much higher than that of 0.5 J/cm^2, leading to higher energy consumption in overcoming air resistance. Due to the sustained energy supply, the attenuation rate of the velocity in the case of 1.2 J/cm^2 was the same as that of 0.5 J/cm^2.

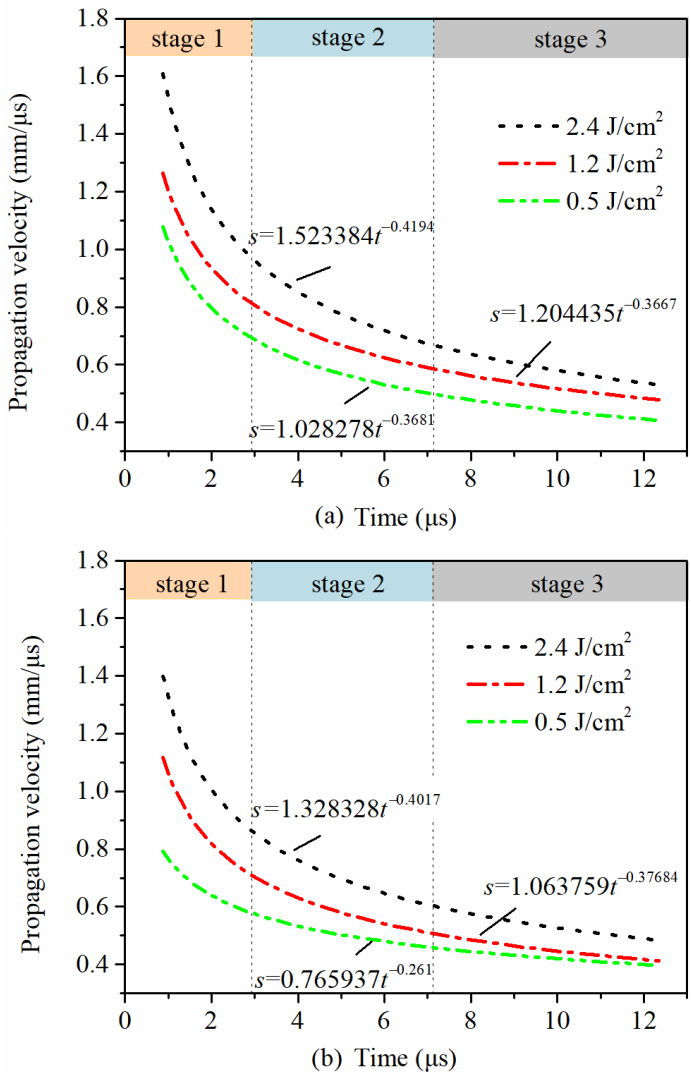


Figure 9. Variations of the propagation velocities of the sub-mAl@GAP (**a**) and sub-mAl (**b**) shock waves with time at different laser fluences.

To make a comparison, variations of the propagation velocities of sub-mAl shock waves with time at different laser fluences are presented in Figure 9b. The evolution history of velocity was also divided into three stages according to Figure 9a. In the first stage, the velocity differences between adjacent laser fluences were totally opposite to that of the sub-mAl@GAP. Additionally, the velocity difference between two samples under 0.5 J/cm^2 gradually decreased over time and tended to be the same in the end. The significant difference between sub-mAl and sub-mAl@GAP was due to the velocity of sub-mAl under 0.5 J/cm^2, which was lower than that of the sub-mAl@GAP in the first stage. With the laser fluence reduced to 0.5 J/cm^2, the energy supporting the shock wave would be mainly contributed by the chemical reaction. Therefore, the velocity of the shock wave from the sub-mAl@GAP was higher than that from sub-mAl owing to an improvement in the energy release by the GAP.

In addition, for both cases, the propagation velocities of the shock waves gradually decreased over time. This was because the energy in the shock wave would be consumed by overcoming the air resistance. The higher the propagation velocity, the greater the air resistance and energy consumption. The propagation velocity of the sub-mAl@GAP was higher than that of sub-mAl, indicating a higher energy release rate of the former than that of the latter. With the increase in the laser fluence, the velocity difference between them went through a history of ups and downs. This reflected that the contribution of

the GAP to the energy release was not linearly related to the laser fluence. The velocity difference between them was the largest under a laser fluence of 1.2 J/cm^2, indicating the largest difference between them in the energy release rate. This was because the energy contribution from the GAP was improved with a temperature rise behind the shock wave front when the laser fluence was over 1.2 J/cm^2. With the increase in the laser fluence from 1.2 J/cm^2 to 2.4 J/cm^2, the energy absorbed by plasma became considerably higher than that from a GAP reaction. Therefore, the propagation of the shock wave mainly relied on the energy absorbed by Al plasma, which led to an attenuation in the velocity difference for them. Despite that, the energy contribution from the GAP was still noticeable. Based on the above analyses, it could be inferred that a GAP coating could improve the energy release rate of the sub-mAl@GAP. The boosting effect of the GAP was particularly remarkable under a low laser fluence.

4. Conclusions

The influence of the GAP on the thermal kinetics and energy release performance of the sub-mAl particles were studied in the work. The thermal analyses on the sub-mAl@GAP revealed that the interaction between the GAP and sub-mAl could benefit the decomposition of the GAP and the oxidation of sub-mAl. The energy release performances of the sub-mAl@GAP under high heating rates were evaluated by means of an electric explosion and a solid laser. In the case of an electric explosion stimulus, the reaction of the sub-mAl@GAP was much more violent than that of sub-mAl. Additionally, the sub-mAl@GAP finished the reaction 0.4 ms earlier than sub-mAl. The energy release performances of the sub-mAl@GAP and sub-mAl under a laser stimulus were conducted with three laser fluences (0.5 J/cm^2, 1.2 J/cm^2, and 2.4 J/cm^2). With the decrease in the laser fluence, the energy contribution of the GAP would be more significant. The Al would ionize under a laser fluence higher than 1.2 J/cm^2. The distance and velocity differences of shock waves generated from the sub-mAl@GAP and sub-mAl were the biggest in the beginning for a laser fluence of 0.5 J/cm^2. The shock wave energy under a laser fluence of 0.5 J/cm^2 would be mainly contributed by the chemical reaction. In this case, the shock wave velocity of the sub-mAl@GAP was higher than that of sub-mAl due to the energy contribution of the GAP to the system. Our work provides new insights into the reaction performance of sub-mAl particles under ultrafast heating rates, benefitting their further modification and application in the explosives.

Supplementary Materials: The following supporting information can be downloaded at: https://www.mdpi.com/article/10.3390/met14070786/s1, Figure S1: Diagram for the laser-Schlieren system; Table S1: Physical and chemical properties of the materials.

Author Contributions: Conceptualization, methodology, formal analysis, investigation, and writing—original draft preparation, Y.L.; resources and data curation, H.R.; data curation and writing-review and editing, S.L. All authors have read and agreed to the published version of the manuscript.

Funding: This research was funded by the Excellent Discipline Cultivation Project by JHUN, grant number 2023XKZ042.

Data Availability Statement: The original contributions presented in the study are included in the article/supplementary material, further inquiries can be directed to the corresponding author.

Conflicts of Interest: The authors declare no conflicts of interest.

Dual-Use Research Statement: We have made the following statements to our paper titled "Influence of GAP on energy release of aluminum sub-micron particles under ultrafast heating rates stimulated by electric explosion and solid laser".

Explanation of Potential Risks: Our paper examines the energy release effect of GAP-modified aluminum sub-micron particles. The research is limited to providing some theoretical and experimental support for the development of chemical dynamics only and does not pose a threat to public health or national security.

Evaluation of Benefits to the General Public: Our research is limited to the academic field, which is beneficial to the development of material science. There is no risk to the general public.

Compliance with Laws: As an ethical responsibility, we strictly adhere to relevant national and international laws about dual-use research. We have considered and adhered to these regulations in our paper.

References

1. Liu, D.Y.; Zhao, P.; Chan, S.H.Y.; Hng, H.H.; Chen, L. Effects of nano-sized aluminum on detonation characteristics and metal acceleration for RDX-based aluminized explosive. *Def. Technol.* **2021**, *17*, 327–337. [CrossRef]
2. Elbasuney, S.; Zaky, M.G.; Bennaya, M.; Abdelkhalek, S.M. The potentials of aluminium nanoparticles: Novel high energy density material for underwater explosions. In *IOP Conference Series: Materials Science and Engineering*; IOP Publishing: Bristol, UK, 2020; Volume 975, p. 012008.
3. Cao, W.; Zhang, X.; Jia, Y.; Zhou, Z.; Li, W.; Xiao, Q.; Xu, S.; Jiao, F.; Zhao, F.; Xu, S. Energy output characteristics and safety design of Al-AlH3 composite dust for energetic material additive. *Combust. Flame* **2023**, *254*, 112842. [CrossRef]
4. Mao, Y.; Chen, J.; Wang, J.; Cao, W.; Wang, J.; Nie, F. Rapid assembly of multilayer nanostructured FG/Al energetic materials to obtain high combustion reactivity. *Chem. Eng. J.* **2023**, *473*, 145302. [CrossRef]
5. Ruesch, M.D.; Mathews, G.C.; Tancin, R.J.; Son, S.F.; Goldenstein, C.S. Wavelength-modulation spectroscopy in the mid-infrared for temperature and HCl measurements in aluminum-lithium composite-propellant flames. *Combust. Flame* **2022**, *242*, 112180. [CrossRef]
6. Wang, J.; Qu, Y.; Gong, F.; Shen, J.; Zhang, L. A promising strategy to obtain high energy output and combustion properties by self-activation of nano-Al. *Combust. Flame* **2019**, *204*, 220–226. [CrossRef]
7. Hu, H.; Chen, L.; Yan, J.; Feng, H.; Xiao, C.; Song, P. Effect of aluminum powder on underwater explosion performance of CL-20 based explosives. *Propellants Explos. Pyrotech.* **2019**, *44*, 837–843. [CrossRef]
8. Ye, M.; Zhang, S.; Liu, S.; Han, A.; Chen, X. Preparation and characterization of pyrotechnics binder-coated nano-aluminum composite particles. *J. Energetic Mater.* **2017**, *35*, 300–313. [CrossRef]
9. Zhang, L.; Li, X.; Wang, S.; Su, X.; Zou, M. Facile energetic fluoride chemistry induced organically coated aluminum powder with effectively improved ignition and combustion performances. *J. Therm. Anal. Calorim.* **2023**, *148*, 1–10. [CrossRef]
10. Zhang, W.; Fan, Z.; Shu, Y.; Ren, P.; Liu, P.; Li, L.K.; Ao, W. Investigation of aluminum particle ignition dynamics in various propellant environments. *Aerosp. Sci. Technol.* **2024**, *149*, 109164. [CrossRef]
11. Zhao, Y.; Cao, W.; Huang, F.; Han, Y.; Long, X. Evaluation of detonation performance and working capacity of explosives by optimized VLW EOS. *Combust. Flame* **2022**, *235*, 111734. [CrossRef]
12. Wang, S.; Yang, Y.; Yu, H.; Dlott, D. Dynamical effects of the oxide layer in aluminum nanoenergetic materials. *Propellants Explos. Pyrotech.* **2010**, *30*, 148–155. [CrossRef]
13. Yang, K.; Chen, L.; Lu, J.; Geng, D.; Wu, J. Reaction mechanism of aluminum nanoparticles in explosives under high temperature and high pressure by shock loading. *Phys. Chem. Chem. Phys.* **2022**, *24*, 14552–14565. [CrossRef] [PubMed]
14. Cook, M.A.; Filler, A.S.; Keyes, R.T.; Partridge, W.S.; Ursenbach, W. Aluminized explosives. *J. Phys. Chem.* **1957**, *61*, 189–196. [CrossRef]
15. Zaiqing, X.; Gengguang, X.; Tingzeng, W.; Yunjian, L. By use of KHT equation of state to calculate detonation parameters of explosives. *Explos. Shock. Waves* **1998**, *18*, 172–176.
16. Strømsøe, E.; Eriksen, S. Performance of high explosives in underwater applications. Part 2: Aluminized explosives. *Propellants Explos. Pyrotech.* **1990**, *15*, 52–53. [CrossRef]
17. Zhang, C.; Lin, B.Q.; Li, W.X.; Zhai, C.; Zhu, C.J. Comparative experimental study on explosion characteristics of nano-aluminum powder and common aluminum powder in the explosive device of a long pipeline. *Adv. Mater. Res.* **2012**, *341*, 113–118. [CrossRef]
18. Elbasuney, S.; Zaky, M.G.; Radwan, M.; Maraden, A.; Abdelkhalek, S.M. Aluminium nanoparticles: The potentials of metalized explosives with combined destructive effect (combustion/detonation). In *IOP Conference Series: Materials Science and Engineering*; IOP Publishing: Bristol, UK, 2020; Volume 975, p. 012009.
19. Zeng, C.; Wang, J.; He, G.; Huang, C.; Yang, Z.; Liu, S.; Gong, F. Enhanced water resistance and energy performance of core-shell aluminum nanoparticles via in situ grafting of energetic glycidyl azide polymer. *J. Mater. Sci.* **2018**, *53*, 12091–12102. [CrossRef]
20. Zeng, C.; Gong, F.; Liu, S. Effect of Al@GAP Composite Particles on Thermal Decomposition Performance of LLM-105. *Chin. J. Explos. Propellants* **2017**, *40*, 27–32.
21. Lima, R.J.P.; Dubois, C.; Stowe, R.; Ringuette, S. Enhanced reactivity of aluminum powders by capping with a modified glycidyl azide polymer. *Int. J. Energetic Mater. Chem. Propuls.* **2016**, *15*, 481–500. [CrossRef]
22. Li, Y.; Ren, H.; Wu, X. Storage stability of glycidyl azide polymer in-situ coating aluminum nanoparticles. *Chin. J. Explos. Propellants (Huozhayao Xuebao)* **2021**, *44*, 839–843.
23. Yudasaka, M.; Kokai, F.; Takahashi, K.; Yamada, R.; Sensui, N.; Ichihashi, T.; Iijima, S. Formation of single-wall carbon nanotubes: comparison of CO_2 laser ablation and Nd:YAG laser ablation. *J. Phys. Chem. B* **1999**, *103*, 3576–3581. [CrossRef]
24. Wainwright, E.R.; Dean, S.W.; Lakshman, S.V.; Weihs, T.P.; Gottfried, J.L. Evaluating compositional effects on the laser-induced combustion and shock velocities of Al/Zr-based composite fuels. *Combust. Flame* **2020**, *213*, 357–368. [CrossRef]

25. Gottfried, J.L.; Dean, S.W.; Collins, E.S.; Wu, C.-C. Estimating the relative energy content of reactive materials using nanosecond-pulsed laser ablation. *MRS Adv.* **2018**, *3*, 875–886. [CrossRef]
26. Gottfried, J.L.; Klapötke, T.M.; Witkowski, T.G. Estimated detonation velocities for TKX-50, MAD-X1, BDNAPM, BTNPM, TKX-55, and DAAF using the laser-induced air shock from energetic materials technique. *Propellants Explos. Pyrotech.* **2017**, *42*, 353–359. [CrossRef]
27. Zhigalin, A.; Rousskikh, A.; Oreshkin, V.; Chaikovsky, S.; Ratakhin, N.; Kuznetsov, V. Experimental research of the fine foil explosion dynamics. *J. Phys. Conf. Ser.* **2014**, *552*, 012027. [CrossRef]
28. Gathers, G. Thermophysical properties of liquid copper and aluminum. *Int. J. Thermophys.* **1983**, *4*, 209–226. [CrossRef]
29. Breitling, D.; Schittenhelm, H.; Berger, P.; Dausinger, F.; Huegel, H. Shadowgraphic and interferometric investigations on Nd: YAG laser-induced vapor/plasma plumes for different processing wavelengths. *Appl. Phys. A* **1999**, *69*, S505–S508. [CrossRef]
30. Kissinger, H.E. Reaction kinetics in differential thermal analysis. *Anal. Chem.* **1957**, *29*, 1702–1706. [CrossRef]
31. Ozawa, T. Kinetic analysis of derivative curves in thermal analysis. *J. Therm. Anal.* **1970**, *2*, 301–324. [CrossRef]
32. Mckay, J.A.; Bleach, R.D.; Nagel, D.J.; Schriempf, J.T. Pulsed-CO_2-laser interaction with aluminum in air: Thermal response and plasma characteristics. *J. Appl. Phys.* **1979**, *50*, 3231–3240. [CrossRef]
33. Nánai, L.; Hevesi, I. Time-resolved spectral investigations of laser light induced microplasma. *Spectrochim. Acta Part A Mol. Spectrosc.* **1992**, *48*, 19–24. [CrossRef]
34. Miller, K.K.; Gottfried, J.L.; Walck, S.D.; Pantoya, M.L.; Wu, C. Plasma surface treatment of aluminum nanoparticles for energetic material applications. *Combust. Flame* **2019**, *206*, 211–213. [CrossRef]
35. Harilal, S.; Bindhu, C.; Tillack, M.; Najmabadi, F.; Gaeris, A. Internal structure and expansion dynamics of laser ablation plumes into ambient gases. *J. Appl. Phys.* **2003**, *93*, 2380–2388. [CrossRef]

Disclaimer/Publisher's Note: The statements, opinions and data contained in all publications are solely those of the individual author(s) and contributor(s) and not of MDPI and/or the editor(s). MDPI and/or the editor(s) disclaim responsibility for any injury to people or property resulting from any ideas, methods, instructions or products referred to in the content.